Filamentary structures that self-organize due to adhesion

A. Sengab and R. C. Picu

Phys. Rev. E **97**, 032506 — Published 23 March 2018

DOI: 10.1103/PhysRevE.97.032506

Filamentary structures self-organized due to adhesion

A. Sengab and R.C. Picu[1]

Department of Mechanical, Aerospace and Nuclear Engineering, Rensselaer Polytechnic Institute, Troy, NY 12180

Abstract

We study the self-organization of random collections of elastic filaments that interact adhesively. The evolution from an initial fully random quasi-two-dimensional state is controlled by filament elasticity, adhesion and inter-filament friction, and excluded volume. Three outcomes are possible: the system may remain locked in the initial state, may organize into isolated fiber bundles, or may form a stable, connected network of bundles. The range of system parameters leading to each of these states is identified. The network of bundles is sub-isostatic and is stabilized by pre-stressed triangular features forming at bundle-to-bundle nodes, similar to the situation in foams. Inter-fiber friction promotes locking and expands the parametric range of non-evolving systems.

[1] Corresponding author. Tel: 1 518 276-2195, E-mail: picuc@rpi.edu.

1. Introduction

Fibrous materials are ubiquitous in biology and the non-living world. Examples of athermal networks (whose fiber mechanics is independent of thermal fluctuations) include the extracellular matrix, connective tissue, paper and non-wovens. The mechanics of such networks was studied extensively [e.g 1,2]. Network models were also used to represent the behavior of granular materials [3], open cell cellular structures [4] and glasses [5].

Most studies to date refer to cross-linked [e.g. 1,2,6] and non-cross-linked [e.g. 7,8] networks whose mechanics is controlled by the fiber properties (fiber bending, $E_f I_f$, and axial, $E_f A_f$, rigidities), network density, ρ, and the mean coordination number, $\bar{z}$. In this work we study non-cross-linked networks in which filaments interact adhesively. Their behavior is qualitatively different from that of other non-cross-linked structures since adhesion re-organizes the network.

This problem is relevant for a broad range of systems. Colloidal interactions produce aggregation in particle suspensions [9]. Suspensions of filaments, whether rigid or flexible, undergo flocculation as the concentration increases and/or the temperature decreases. The formation of filament bundles, followed by organization into a network of bundles was observed in dense suspensions of actin [10] and collagen [11], and was discussed theoretically in [12].

Carbon nanotubes (CNT) interact adhesively and form bundles, which further self-organize into networks of bundles [13,14]. Buckypaper [14] is entirely stabilized by inter-CNT adhesion. The structure of CNT assemblies depends on the bending stiffness of filaments [15], the CNT length [16] and, in single-wall CNTs, on bending buckling of CNTs [17]. Buckypaper can be stretched to produce CNT yarns, which may replace carbon fiber in structural composites [18]. The viscoelastic behavior of such CNT structures is temperature independent, which demonstrates their athermal nature [19].

Fibrils can be brought together into bundles [20] and larger structures [21,22] by surface forces which are longer ranged than adhesion, such as capillary forces. Elastocapillarity controls the interaction of liquid-air and liquid-liquid interfaces with elastic structures and produces self-organization effects similar to those associated with adhesion and discussed here [23,24].

In this work we study the effect of adhesion on the structure of non-crosslinked networks of filaments which are free to move relative to each other. We observe that adhesion drives fiber

bundling. We investigate the types of structures that result upon filament bundling and the dependence of the resulting configurations on network parameters. We also study the effect of inter-fiber friction on the onset of the self-organization process. The results indicate the range of controllable network parameters that lead to each of the various types of self-organized structures observed both in presence and in absence of inter-fiber friction.

2. Models and methods

To study the effect of adhesion on non-crosslinked fibrous assemblies, we use the bead-spring model of polymer physics [15,16,20]. The axial and bending stiffness of filaments are represented by harmonic potentials defined by their respective constants, $k_a = E_f A_f / s_0$ and $k_b = E_f I_f / s_0$, where s_0 is the distance between consecutive beads along the filament, and E_f,A_f, I_f are the fiber elastic modulus, cross-section area and moment of inertia. Fibers have zero torsional stiffness. This is not a limitation since it is known that very little strain energy is stored in the torsional mode of fibers in random fiber networks [1]. In addition, curling would be observed in simulations if the system would store energy in the torsion mode. All fibers in the model have same length, L_0, same diameter, d_0, and E_f. All fibers have circular cross-section.

Non-bonded interactions are represented with a Lennard-Jones potential of characteristic length $\sigma$and energy parameter ε_0. The potential imposes the excluded volume constraint and models the inter-fiber adhesion. The work of adhesion, γ, results as the interaction energy per unit length of contact between two parallel, straight fibers in equilibrium.

Some level of inter-fiber friction is caused by the roughness of filaments associated with the discrete nature of the bead-spring representation. To minimize this effect, we increase the density of beads along each filament to 4 beads per fiber segment of aspect ratio 1, i.e. $s_0 = d_0/4$. It was determined using pairs of parallel filaments in adhesive contact forced to slide against each other axially that, with this axial bead density, the fluctuation of the adhesive energy per unit length of filament is only 0.01% of the mean value.

The three fiber parameters, γ, d_0 and E_f are uniquely defined by the model parameters σ, ε_0 and k_a. Parameter d_0 is the equilibrium distance of a bead from the axis of an infinite straight

fiber and, for the potentials used, it is $d_0 = 1.063\sigma$. Parameter $\gamma$is given by $\gamma = 7.11\varepsilon_0/\sigma$. The effective fiber modulus is defined by k_a as $E_f = 0.3k_a/\sigma$.

The initial, "as-deposited" configuration of the model is generated by depositing fibers of length L_0 on a non-frictional support plane, in an area of size L x L, with $L > 2L_0$ in all cases such to avoid spurious effects introduced by the periodic boundary conditions. Newly deposited fibers lay on top of the previously deposited ones without interpenetration, forming a quasi-two-dimensional mat structure. Adhesive interactions at contacts insure that the mat retains integrity during fiber deposition. Periodic boundary conditions are imposed in the plane of the mat during deposition, while traction free (vacuum padding) conditions are applied in the direction perpendicular to the mat.

The as-deposited structures of fibers have random orientations and random positions of their centers of mass. It is convenient to describe the initial structure in projection on the support plane, projection in which the network resembles a Mikado structure [2,6] characterized by its density (total fiber length per unit area), ρ, and the fiber length, L_0. The density has units of 1/length and is related to the mean segment length of the network (segment between two contacts) by the Kallmes-Corte relation $l_c = \pi/2\rho$ [25]. We note that the quasi-two-dimensional assumption is valid if the mat is sufficiently thin and fibers are sufficiently flexible for the newly deposited fibers to make contact with all previously deposited fibers on top of which they fall. A conceptual perspective on this issue is discussed in [26]. Once the mat is deposited, the support plane is removed and the structure is relaxed at fixed L, by imposing periodic boundary conditions in the plane of the mat and zero tractions in the direction perpendicular to the mat. The system does not disintegrate by diffusion in the out-of-plane direction due to the adhesion between fibers. Further, the system is evolved with molecular dynamics under the same boundary conditions, which represent a system of infinite in-plane extent and of constant density.

In separate simulations we study the effect of static friction between filaments on the onset of adhesion-driven self-organization. To this end, an additional attractive potential of well depth ε_f is introduced between beads belonging to different fibers, at contacts between filaments in the initial network configuration. In absence of this interaction the relative sliding of fibers is frictionless since the adhesion energy remains constant. These "stickers" introduce resistance to the onset of sliding and an effective maximum unbinding force proportional to ε_f/d_0. This model does not represent dissipative Coulomb friction, rather it is designed to model static

friction between fibers in contact in the as-deposited state. It is used only to determine whether adhesion is strong enough to initiate fiber re-arrangement for given ε_f.

3. Results and discussion

3.1 Structural evolution and stabilization of cellular networks of bundles

In general, the as-deposited system of filaments may be locked in the initial configuration or may evolve due to the adhesive forces. Evolving systems self-organize into cellular structures of filament bundles or disintegrate forming largely disconnected filament bundles. Figs. 1(a) and 1(b) show the initial and final stages of an evolution that transforms a Mikado-like initial structure, into a cellular structure of filament bundles. A movie showing this evolution is presented in the Supplementary material [27]. The movie shows the view perpendicular to the plane of the as-deposited mat, similar to Fig. 1.

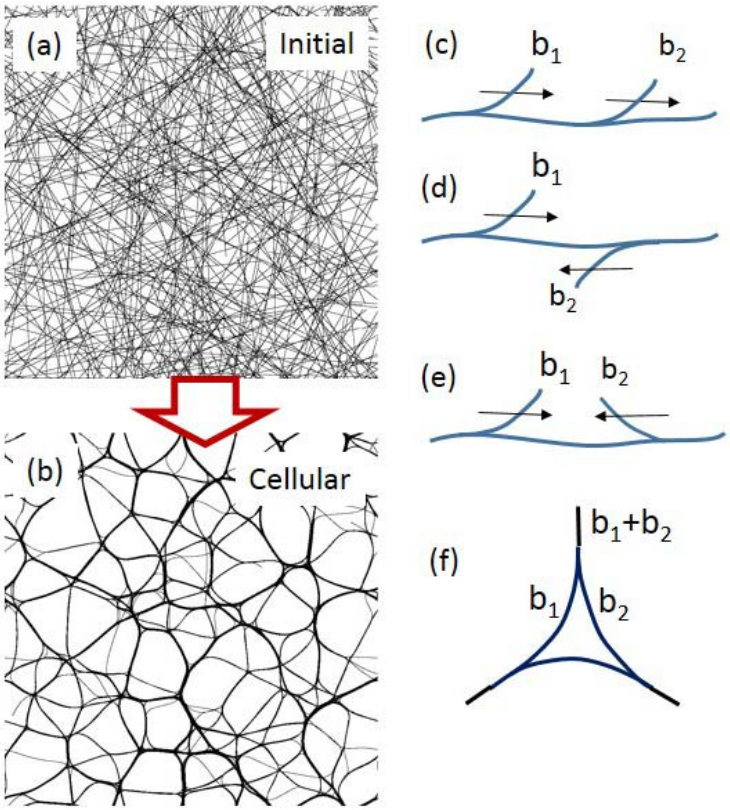

FIG. 1. Evolution of a network due to fiber adhesion from an initial structure (a) into a cellular network of bundles (b). Bundles may merge to form larger bundles (c), may pass each other without interacting (d), or may interact forming triangular features (e), such as that in (f).

A cellular structure of filament bundles (Fig. 1(b)) is a qualitatively different stochastic network which has not been studied so far. In the 2D projection it resembles a Voronoi tessellation and all nodes have coordination $z = 3$. All network segments are bundles stabilized by the adhesive interaction of filaments. Bundles split into two sub-bundles at a node. Nodes can move along a segment by bundling or un-bundling. Fig. 1(c) shows three bundles forming two nodes. Bundles b_1 and b_2 are shown moving in the same direction; they may eventually merge into a larger bundle. If b_1 and b_2 move in opposite directions, they can pass each other without interaction (Fig. 1(d)) or interact (Fig. 1(e)) forming a triangular feature, Fig. 1(f). These triangles are stabilized by the adhesion between bundles and store strain energy.

To study the effect of network parameters on the self-organized network structure, systems with multiple values of these parameters are considered and are evolved. The relevant system parameters are γ, E_f, L_0, d_0 and ρ. Consider first that the inter-filament friction vanishes. The Buckingham π analysis indicates that three independent non-dimensional groups can be formed from this set: e.g. $\xi_1 = \gamma/E_f d_0^2$, $\xi_2 = \rho L_0$, and $\xi_3 = L_0/d_0$. We consider 24 combinations of these parameters and simulate all corresponding systems. Fig. 2 shows the points corresponding to these configurations in the ξ_1, ξ_2, ξ_3 space. We observe three types of structures which are represented in Fig. 2 by the three types of symbols. The crosses correspond to configurations that do not evolve and remain in the as-deposited state. Filled squares indicate configurations that evolve into stable cellular structures similar to that shown in Fig. 1(b). The open circles indicate networks which disintegrate and hence lose connectivity. The plane shown in Fig. 2 separates the non-evolving from the evolving structures and is defined by $\xi_1 \xi_3^2 = a' \xi_2^2$. The functional form of this surface is motivated by considerations presented below. This representation suggests that the relevant physics can be described in a space with two dimensions in which this separation plane is viewed edge-on and appears as a line (Fig. 3). The parameters of this space of reduced dimensionality are $\log_{10}(\xi_2)$ and $\log_{10}(\Psi) = \log_{10}(\xi_1) + 2\log_{10}(\xi_3)$, i.e. $\Psi = \xi_1 \xi_3^2 = \gamma L_0^2/E_f d_0^4 \sim \gamma L_0^2/E_f I_f$. The $\log_{10}(\xi_2)$ axis, $\log_{10}(\Psi)$ axis (which is perpendicular to $\log_{10}(\xi_2)$), and the normal to the separation plane are coplanar. The $\log_{10}(\Psi)$ - $\log_{10}(\xi_2)$ frame is shown schematically in Fig. 2.

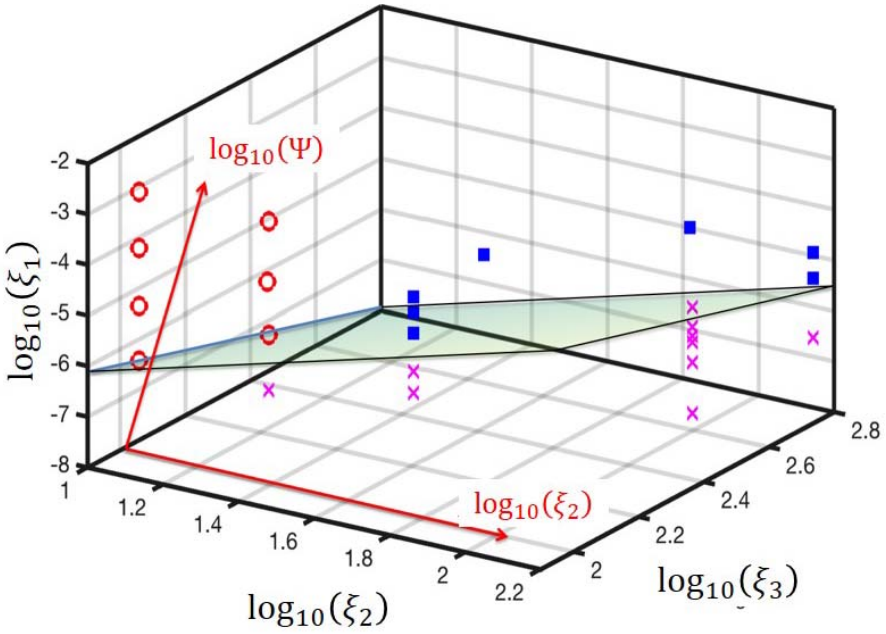

FIG. 2. Systems without inter-fiber friction considered in simulations shown in the space of non-dimensional system parameters. The frame $\log_{10}(\Psi)$ - $\log_{10}(\xi_2)$ used to represent the data in Fig. 3 is shown schematically in red.

Parameter Ψ can be rewritten as $\Psi = L_0^2/L_{EC}^2$, where L_{EC} is the elastocapillarity length introduced in [23]. It captures the physics of bending-dominated elasticity in presence of adhesive forces [28] and was used in [16,20] to analyze CNT structures. Ψ shows that strong adhesion effects result by increasing γ and by decreasing the filament diameter. Since $I_f \sim d_0^4$, decreasing d_0 has a stronger effect than increasing γ, which explains why adhesion effects are generally observed with nanofibers [20].

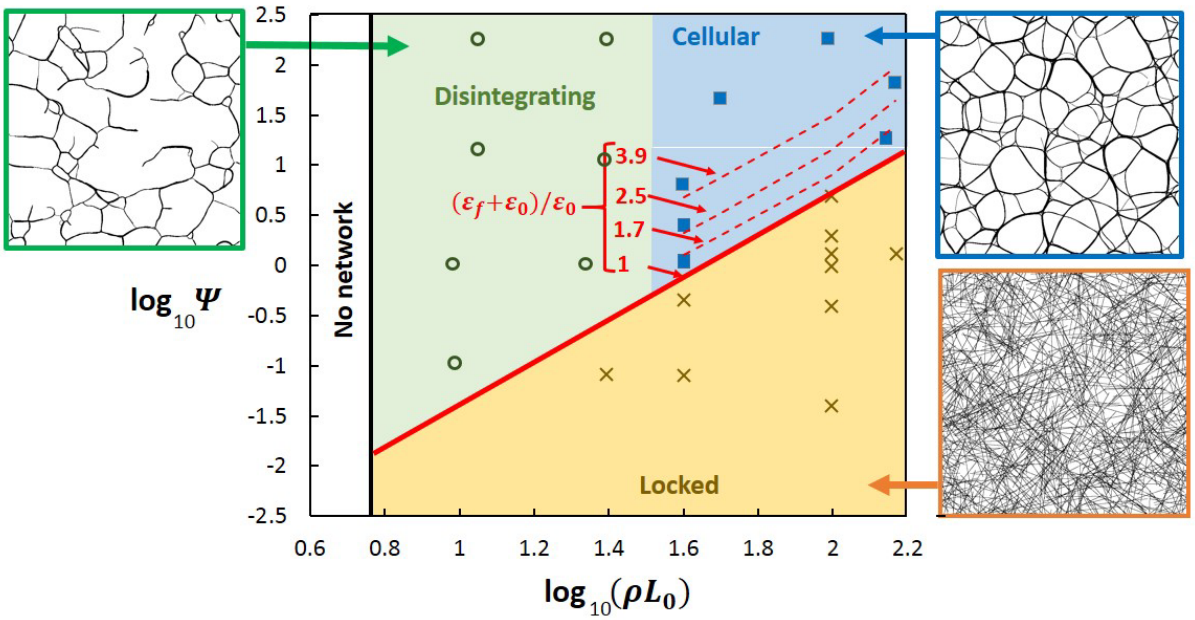

FIG. 3. (color online). Map of three possible network states in the plane of non-dimensional parameters $\Psi = \gamma L_0^2/E_f I_f$ and ρL_0. For $\rho L_0 < 5.71$, the initial network is below the percolation threshold. The small Ψ domain labeled "locked" corresponds to structures that do not evolve from the initial state and hence do not bundle. This domain is bounded above by the red line of equation $\Psi \sim (\rho L_0)^2$ which is a particular form of eq. (2) corresponding to the no inter-fiber friction case. In presence of friction (quantified by parameter ε_f) this boundary moves up, as shown by the set of dashed red lines (eq. 2). For larger Ψ values, systems self-organize in networks of fiber bundles (Fig. 1(b)) which are stabilized by triangular features forming at network nodes (Fig. 1(f)). At low ρL_0 these structures loose connectivity and the network disintegrates. The crosses, open circles and filled squares indicate cases simulated that lead to locked, disintegrated and cellular structures, respectively. The side panels show examples of the three types of structures described.

Figure 3 presents the results in the frame $\log_{10}(\Psi)$ - $\log_{10}(\rho L_0)$ parametric space. For $\rho L_0 \leq 5.71$, the initial state is not a percolated network [29] and hence the present problem is not defined. This threshold corresponds to the sol-gel transition observed in thermal suspensions of nanorods [12].

For $\rho L_0 > 5.71$ and small Ψ, systems do not evolve from the as-deposited state and no bundles develop. To understand this situation, consider the initial stage of relaxation at the scale of two crossed filaments forming an angle α in the initial state. To enable adhesion (short range interaction), the filaments have to bend towards each other by $\alpha/2$ at the crossing point. The energy gained is γy, where y is the length of the resulting segment in contact. The strain energy stored in the deforming filaments and the work done against the background friction (if any) are the energy expenditures. The rotation and sticking of filaments in the vicinity of the contact point must be accommodated either by their axial deformation or by sliding along their contour, which happens against the friction forces acting at all contacts of the respective filament with other filaments. To evaluate the bending energy, consider a filament segment of length l_c ($l_c = \pi/2\rho$ [25]) which rotates by $\alpha/2$ at both ends, allowing adhesion with contacting filaments at both ends. The bending energy stored is $u_b = E_f I_f \alpha^2/2l_c$. The work performed against friction at contact points along the filament is the fiction force, F_f, assumed to be identical at all contacts, times the number of contacts, $\sim L_0/2l_c$, and times the relative sliding distance of the two filaments required by the rotation at contact points: $w_f \sim L_0 F_f \alpha^2$. Therefore, the average of the sum of the bending energy and work per filament is

$$\bar{u}_b + \bar{w}_f = \frac{E_f I_f}{L_0}\left(a(\rho L_0)^2 + b\rho L_0 \Psi_f\right)\overline{\alpha^2}, \qquad (1)$$

where a and b are coefficients of order unity and $\Psi_f = F_f L_0^2/E_f I_f$ represents the contribution of inter-filament friction. For bundling to proceed, the energy gain per filament $\gamma L_0 \overline{y/L_0}$ must be larger than the energy stored and dissipated. Treating the normalized mean sticking length per filament, $\overline{y/L_0}$, as a constant smaller than 1, the condition for the onset of system self-organization becomes:

$$\Psi > a'(\rho L_0)^2 + b'\rho L_0 \Psi_f. \qquad (2)$$

The relation $\Psi \sim (\rho L_0)^2$ corresponding to the no friction case ($\Psi_f = 0$) is shown in Fig. 3 as the red line bounding above the domain labeled "locked" and in Fig. 2 as the surface separating locked and evolving structures. The crosses shown in Figs. 2 and 3 represent simulated configurations that remain locked in the initial, "as-deposited" state ($\Psi_f = 0$).

The upper region of the map in Fig. 3 corresponds to evolving structures. At low ρL_0 the network disintegrates, while self-organized networks of bundles form at larger ρL_0. The boundary between these two regimes cannot be predicted analytically and is defined

approximately based on simulation results. Models with $\Psi_f = 0$ and various sets of parameters are considered and are evolved until stabilization or disintegration. These cases are shown in Figs. 2 and 3 with symbols indicating the final state of the system: open circles and filled squares correspond to disintegrating and cellular structures, respectively. The side panels of Fig. 3 show examples of each structure type.

Increasing the fiber length L_0 moves any point in the map parallel to the boundary between locked and evolving structures, into the cellular range. Increasing the density ρ at constant L_0 moves the point to the right. Therefore, cellular structures can be obtained at given γ by working with filaments of smaller diameter and larger length, while keeping friction to a minimum.

The results in Fig. 3 apply to a number of nano-fiber systems in which adhesion is important. The vertical axis parameter Ψ refers to the fiber properties, while the horizontal axis parameter ρL_0 refers to the network. Keeping ρ and L_0 arbitrary, it is only possible to compare material systems based on their L_{EC}; note that $\Psi \sim L_{EC}^{-2}$ and $L_{EC} = \sqrt{E_f I_f / \gamma}$. Parameter γ was measured [30] for pairs of double wall carbon nanotubes of 2.2 nm diameter to the 1.7 nN. Estimates for hydroxyl functionalized carbon nanotubes (CNT) and for carbonyl functionalized CNTs are 0.13 nN and 0.24 nN, respectively [30]. The bending rigidity of CNTs does not depend strongly on chirality, but varies significantly with the nanotube diameter. For a diameter of 2.2 nm, $E_f I_f \approx 880$ nN nm^2, while for single wall nanotubes of 0.4 nm diameter, which are circular in cross-section, $E_f I_f \approx 160$ nN nm^2 [31]. These values lead to L_{EC} in the range 20 to 40 nm. This very small value of L_{EC} indicates strong adhesion, which is expected for CNT-CNT interaction. Another example is provided by microtubules for which the inter-tube adhesion was measured function of the ionic strength of the solution to be in the range 2×10^{-5} to 17×10^{-5} nN [32]. With $E_f I_f = 2 \times 10^4$ nN nm^2 [33], L_{EC} results in the range 10 to 30 μm.

We observe that cellular structures stop evolving once triangles of fiber bundles form at all cell nodes (Figs. 1(b) and 1(f)). These resemble the Plateau triangles known in the physics of foams [34]. Plateau triangles form at each junction of three cell walls in the foam, have curvilinear triangular section and insure the stability of the foam. While Plateau triangles are stabilized by surface tension, the triangular features discussed here are stabilized by the interplay of adhesion and bending.

Consider the triangular structure shown in Fig. 4(a) which represents the node connecting filament bundles AA', BB' and CC', belonging to a larger network. The structure is characterized by the number of filaments in each incoming bundle, n_1, n_2 and n_3, and the three angles, α_1, α_2 and α_3. This structure stores adhesion and bending energy. The axial energy of the filaments vanishes since these are free to relax in the axial direction. The bending energy is stored only in segments AC, AB and BC. All segments store adhesion energy.

The adhesion energy in a bundle of n filaments per unit length of the bundle is given by $E_a = \gamma n_c(n)$, where n_c is the number of binary contacts in the bundle. Harborth [35] has shown that the maximum number of contacts in a packing of n congruent circles is $n_c(n) = 3n - \sqrt{12n-3}$. The bending rigidity of a bundle of n filaments is $nE_f I_f$, since fibers are free to slide axially.

Several observations can be made by inspection. Bundles AB, BC and AC forming the triangle are loaded in pure bending and hence are arcs of circle. Since these circles must be tangent to each other at A, B and C, segments OA, OB and OC are also of equal length. If bundles AA', BB' and CC' are straight, the bending moments loading the three edges of the triangle are equal.

This is a pre-stressed, self-equilibrated structure which can be perturbed only by bending moments applied at A', B' and C'. If segments AA', BB' and CC' are straight, no driving force for the evolution of the triangle exists. In all cellular structures simulated to full relaxation the cell walls become straight (Fig. 1(b)). Hence, the network stores strain energy only in triangles. Figure 4(b) shows a pair of such triangles isolated from one of the cellular structures. To demonstrate its stability, this structure was fully relaxed while applying no tractions at the free ends of bundles, and its configuration remained essentially unchanged. This can be understood considering that the structure in Fig. 4(b) is not loaded by the rest of the network when connected to the structure to which it belongs.

Another possible evolution mode is fiber diffusion along its contour. Reptation is driven here only by the difference in chemical potential between the filament ends. Consider a filament diffusing from B' to C', which would lead to the variation of n_2 and n_3 and hence to the change of the triangle shape. The filament has to bend in region BC, which represents a significant energetic barrier for reptation. Furthermore, mechanically forcing two triangles against each other leads to mutual distortion which requires substantial energy expenditure. We conclude that

cellular networks are stabilized by such triangles and, once the cell walls become straight, the entire network stops evolving.

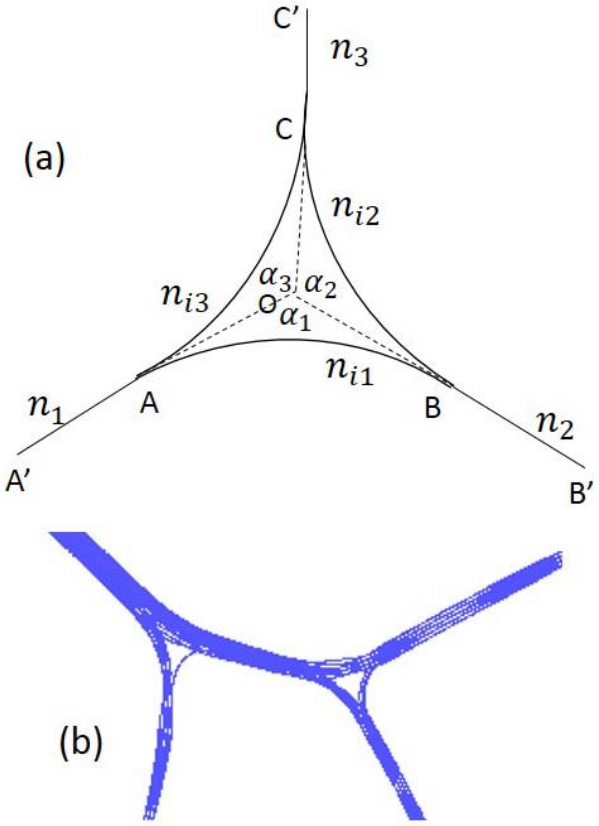

FIG. 4. (a) Triangular structure forming the node connecting bundles AA', BB' and CC' of a larger network. (b) Structure containing 2 triangles isolated from a larger cellular network.

3.2 Effect of inter-fiber friction

Inter-fiber friction has a marked effect on the boundary separating locked and evolving structures. This boundary is defined by simulations in which the initial stages of system evolution are observed. The as-deposited structure is allowed to evolve under the action of adhesion, and the angles between crossing fibers are monitored. If the relative position of fibers at contact points does not change, the system is considered "locked." The boundary shown by the continuous red line in Fig. 3 corresponds to the case with no friction, $\Psi_f = 0$, i.e. $\varepsilon_f = 0$. The

crosses in Fig. 3 indicate cases with $\varepsilon_f = 0$, which were simulated and correspond to locked configurations.

For cases with $\Psi_f > 0$, i.e. $\varepsilon_f > 0$, the boundary moves up; these boundaries are shown with dashed lines in Fig. 3 for several values of ε_f. Figure 5 shows the simulation data points defining the position of the dashed lines in Fig. 3. Three columns of data points are shown for each of three ρL_0 values. These correspond to $(\varepsilon_f + \varepsilon_0)/\varepsilon_0 = 1.7, 2.5, 3.9$ and define the blue, red and green dashed boundaries in Fig. 5, respectively. The columns labeled with the same ρL_0 value are shifted horizontally for clarity. The blue square data point at the top of each column represents an evolving structure corresponding to the respective ρL_0 and $(\varepsilon_f + \varepsilon_0)/\varepsilon_0$. Hence, the dashed lines are positioned between the uppermost cross and the corresponding square data point of each column.

For $\Psi_f > 0$, the boundary is represented by eq. 2: $\Psi = a'(\rho L_0)^2 + b'\rho L_0 \Psi_f$. Rewriting this expression by using the definition of Ψ_f, leads to:

$$\log_{10}\Psi = \log_{10} a' + 2\log_{10}\rho L_0 + \log_{10}\left[1 + c'\frac{\varepsilon_f}{\varepsilon_0}\frac{\Psi}{\rho L_0}\right], \qquad (3)$$

with c' being a numerical coefficient. The last term in eq. (3), $D = \log_{10}\left[1 + c'\frac{\varepsilon_f}{\varepsilon_0}\frac{\Psi}{\rho L_0}\right]$, represents the deviation of the dashed lines in Fig. 5 from the continuous red line (representing $\Psi_f = 0$) for cases with $\varepsilon_f > 0$. For small deviations, $D \approx c'\frac{\varepsilon_f}{\varepsilon_0}\frac{\Psi}{\rho L_0} \approx a'c'\frac{\varepsilon_f}{\varepsilon_0}\rho L_0$, which indicates that $D \sim \varepsilon_f/\varepsilon_0$ and $D \sim \rho L_0$, which agrees with the numerical results shown in Fig. 5.

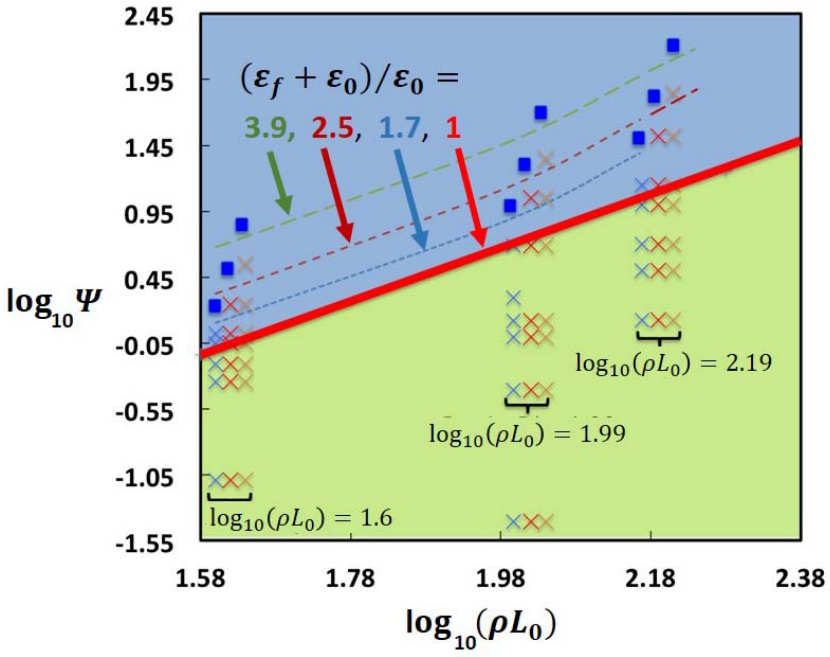

FIG. 5. Data points defining the position of the boundary between locked and evolving structures for cases with inter-fiber friction. For each of the 3 indicated values of ρL_0, the three columns of data correspond to 3 values of $(\varepsilon_f + \varepsilon_0)/\varepsilon_0$, and each defines a boundary shown by the dashed lines. The blue square data point at the upper end of each column shows an evolving structure.

The analysis indicated that inter-filament friction restricts the onset of system evolution. Since $\Psi_f \sim L_0^2$, increasing the filament length at constant F_f (or ε_f) moves this boundary up. This effect is strong and may effectively lock realistic structures in the as-deposited state even at small F_f values.

4. Conclusions

Similar to elasto-capillarity, adhesion drives the self-organization of filamentary structures. In this work we study the structures that result from this process and the effect of inter-fiber friction on self-organization. We observe that if adhesion is weak or/and the bending rigidity of fibers is large (large elasto-capillarity length), the fibrous structure remains locked in the initial configuration. Strong adhesion and/or small fiber bending rigidity promote system evolution. The boundary between locked and evolving structures is defined in terms of a parameter quantifying the inter-fiber friction. Friction expands the parametric domain of locked structures.

Evolving structures either disintegrate or stabilize in the form of cellular networks of fiber bundles. This new type of network is sub-isostatic and is stabilized by triangular features that form at all network nodes. This stabilization mechanism is purely adhesive in nature and does not require inter-fiber friction. These results provide a broad physical picture relevant for a large number of fibrous materials ranging from carbon nanotube networks to biological structures.

Acknowledgment

This work was supported by the NSF through grant CMMI-1634328.

References

[1] C.P. Broedersz and F.C. MacKintosh, Modeling semiflexible polymer networks, Rev. Mod. Phys. **86**, 995 (2014).

[2] R.C. Picu, Mechanics of random fiber networks – a review, Soft Matter **7**, 6768 (2011).

[3] A.J. Liu and S.R. Nagel, Nonlinear dynamics: Jamming is not just cool any more, Nature **396**, 21 (1998)

[4] L. J. Gibson and M. F. Ashby, Cellular solids: structure and properties (Cambridge University Press, Cambridge, 1999).

[5] M. van Hecke, Jamming of soft particles: geometry, mechanics, scaling and isostaticity, J. Phys.: Cond. Mat. **22**, 33101 (2010).

[6] C. Heussinger and E. Frey, Role of architecture in the elastic response of semiflexible polymer and fiber networks, Phys. Rev. E 75, 011917 (2007).

[7] S. Toll, Packing mechanics of fiber reinforcements, Polym. Eng. Sci. **38**, 1337 (1998).

[8] G. Subramanian, R.C. Picu, Mechanics of three-dimensional, non-bonded random fiber networks, Phys. Rev. E **83**, 056120 (2011).

[9] A. Wierenga, A.P. Philipse, H.N. Lekkerkerker, D.V. Boger, Aqueous dispersions of colloidal boehmite: Structure, dynamics, and yield stress of rod gels, Langmuir **14**, 55 (1998)

[10] M. Tempel, G. Isenberg, and E. Sackmann, Temperature-induced sol-gel transition and microgel formation in a-actinin cross-linked actin networks – a rheological study, Phys. Rev. E **54**, 1802 (1996).

[11] S. Yunoki, H. Hatayama, M. Ebisawa, E. Kondo, K. Yasuda, A novel fabrication method to create a thick collagen bundle composed of uniaxially aligned fibrils, J. Biomed. Mater. Res. A **103**, 3054, 2015.

[12] A.G. Zilman, S.A. Safran, Role of cross-links in bundle formation, phase separation and gelation of long filaments, Europhys. Lett. **63**, 139 (2003).

[13] A. Thess, R. Lee, P. Nikolaev, et al., Crystalline ropes of metallic carbon nanotubes. Science **273**, 483 (1996).

[14] L. Berhan, Y. Yi, A. Sastry, E. Munoz, M. Selvidge, R. Baughman, Mechanical properties of nanotube sheets: Alterations in joint morphology and achievable moduli in manufacturable materials. J. Appl. Phys. **95**, 4335 (2004).

[15] Y. Li, M. Kröger, Computational study on entanglement length and pore size of carbon nanotube buckypaper, Appl. Phys. Lett. **100**, 021907 (2012).

[16] Y. Li, M. Kröger, A theoretical evaluation of the effects of carbon nanotube entanglement and bundling on the structural and mechanical properties of buckypaper, Carbon 50, 1793 (2012).

[17] A.N. Volkov, L.V. Zhigilei, Structural stability of carbon nanotube films: the role of bending buckling. ACS Nano **4**, 6187 (2010).

[18] K. Sugano, M. Kurata, H. Kawada, Evaluation of mechanical properties of untwisted carbon nanotube yarn for application to composite materials. Carbon **78**, 356 (2014).

[19] M. Xu, D.N. Futaba, T. Yamada, M. Yumura, K. Hata, Carbon nanotubes with temperature-invariant viscoelasticity from –196 to 1000 C, Science **330**, 1364 (2010).

[20] S. Cranford, H. Yao, C. Ortiz, M.J. Buehler, A single degree of freedom 'lollipop'model for carbon nanotube bundle formation, J. Mech. Phys. Sol. **58**, 409 (2010).

[21] M.A. Correa-Duarte, N. Wagner, J. Rojas-Chapana, C. Morsczeck, M. Thie, M. Giersig, Fabrication and biocompatibility of carbon nanotube-based 3D networks as scaffolds for cell seeding and growth, Nano Lett. **4**, 2233 (2004).

[22] M. De Volder, A.J. Hart, Engineering hierarchical nanostructures by elastocapillary self-assembly, Angew. Chem. Int. Ed. **52**, 2412 (2013).

[23] J. Bico, Elastocapillary coalescence in wet hair, Nature **432**, 690 (2004).

[24] R.W. Style, A. Jagota, C.Y. Hui, E.R. Dufresne, Elastocapillarity: surface tension and the mechanics of soft solids, Annu. Rev. Cond. Mat. Phys. **8**, 99 (2017).

[25] O. Kallmes, H. Corte, The structure of paper, I. The statistical geometry of an ideal two dimensional fiber network. Tappi J. **43**, 737 (1960).

[26] A. Ekman, A. Miettinen, T. Tallinen, J. Timonen, Contact formation in random networks of elongated objects, Phys. Rev. Lett. 113, 268001 (2014).

[27] See supplementary materials at *** for a movie of the structural evolution of a network with $\Psi = 182$, $\rho L_0 = 99.25$ and $\Psi_f = 0$.

[28] J.N. Israelachvili, Intermolecular and surface forces (Academic Press, New York, 1991).

[29] J. Wilhelm, E. Frey, Elasticity of stiff polymer networks. Phys. Rev. Lett. **91**, 108103 (2003).

[30] T. Filleter et al., Nano Letters, **12**, 732 (2012).

[31] X. Guo, T. Zhang, J. Mech. Phys. Sol. **58**, 428 (2010).

[32] F. Hilitski, A.R. Ward, L. Cajamarca, M.F. Hagan, G.M. Grason, Z. Dogic, Phys. Rev. Lett. **114**, 138102 (2015).

[33] F. Gittes, B. Mickey, J. Nettleton, J. Howard, J. Cell Biol. 120, 923 (1993).

[34] D. Weaire, S. Hutzler, The Physics of Foams (Oxford University Press, New York, 1999).

[35] H. Harborth, Solution to problem 664A, Elem. Math **29**, 14 (1974).